INTERNATIONAL JOUNAL OF: ENGINEERING RESEARCH AND TECHNOLOGY

TIMBOU-AFRICA ACADEMIC PUBLICATIONS
INTERNATIONAL JOURNAL, NOVEMBER, 2022 EDITIONS
VOL. 11 NO. 5 ISSN: 2707-5654

STUDY OF OPTICAL PROPERTIES OF HYDROXYAPATITE/TITANIUM DIOXIDE FOCUS: IN BANDGAP ENERGY DETERMINATION USING THREE DIFFERENT MODELS.

***T. YUNANA; **H. ALI; & **M. ONIMISI**

*Department of Physics, Kaduna state College of Education, Gidan Waya, Kaduna State, Nigeria.
**Department of Physics, Nigerian Defence Academy, Kaduna, Kaduna State, Nigeria.

ABSTRACT

In the recent past, improvement of optical and band gap energy properties of photocatalytic materials via the amalgamation of synthetic titanium dioxide with natural mineral modifier became a new strategy to achieve novel photovoltaic optical devices. Inspired by this idea, we prepared a natural minerals called hydroxyapatite ($Ca_{10}(PO_4)6(OH)$

Introduction

Nanocrystal line titanium dioxide (TiO_2) thin films have been investigated extensively in recent years because of their potential use as a low cost material in photovoltaics gas sensors photocatalytic [1-3], smart windows, antireflection coatings, optical filters [4- 6] and as dye-sensitized solar cells [7]. However, literature reported that a wide range of semiconductor photo catalysts such as TiO_2, ZnS, Fe_2O_3, CdS, GaP and ZnO had proven their efficacy by degrading the various organic pollutants in the presence of light by monitoring its band gap energy. [8] Among them, titanium

$_2$) with TiO_2 stochiometrically by standard sol – gel method and characterized. The role of varying percentage weight of HAp on optical and bandgap energy proposed was fully examined. UV –visible spectroscopy was used to measure the absorbance data, were optical constants such as absorption coefficient, extension coefficient, refractive index, transmittance and absorbance were evaluated. From the optical analysis it was found that, the absorption response in UV-region is at 200nm – 400nm with an absorption edge around (650 – 950) nm was achieved, and its transmittance is at (400 – 800) nm in the visible region. The value of absorption coefficient (α) and extension coefficient (k) of HAP/TiO_2 increased with increasing the wt% of HA. likewise, the band gap energy decreases as the percentage weight of HAP increases in all the three models, Notwithstanding, the optical band gap in DASF (derivation of absorption spectrum fitting) method was obtained by taking the whole derivative of the spectrum instead of extrapolating certain range as in Tauc and ASF (absorption spectrum fitting) method. As a result, this makes DASF method exceptional, more efficient and accurate model for band gap energy determination.

Keywords: Hydroxyapatite, titanium dioxide, optical band gap, spectrum fitting, nanoparticles.

dioxide (TiO_2) has gained an interest in photocatalytic wastewater treatment owing to its thermal stability, and its higher chemical resistivity and robust mechanical properties. [9-13]. It was found that, TiO_2 can exist in amorphous form and also in three crystalline forms – anatase (a) rutile (r) and brookite (b). These phases are well distinguishable in terms of their physical properties. anatase and rutile phases are tetragonal in nature. Optical band gap is higher for anatase compared to that of rutile (3.2 vs 3.0 ev). anatase phase is known to

exhibit better photocatalytic activity and is preferred over rutile for photodecomposition of environmental pollutants [14 -16]. Rutile phase exhibits better optical activity than anatase and is used for antireflective and dielectric applications [17,18]. High dielectric constant of the material enables the use of TiO_2 thin films in micro-electronic devices [19]. The variation in properties, exhibited by amorphous, anatase and rutile thin films, have generated much interest in the study of their growth mechanisms and towards the energy band gap determination, Since the optical properties of TiO_2 films also show interesting variations influenced by oxygen defects, impurities and crystalline size. However, utilization of TiO_2 was constrained due to its low adsorption performance for pollutants [20,21] and high recombination of photo generated electron-hole pairs as a result of suggested energy band gap. [22,23]. Moreover, literature suggested that composite introducing of TiO_2 with other materials, such as hydroxyapatite (HAP), zeolite, silica, activated carbon, had evidenced to enhance the sample active adsorption sites, improved band gap energy which may results in rapid mass transfer of mobility carrier from the valence band to the conduction band and ultimately increase the rate of catalytic reactions. [24,25]. Notwithstanding, hydroxyapatite (HAP), $Ca10(PO_4)6(OH)_2$ is having outstanding mechanical stability, good biocompatibility, non-toxicity and less expensive. [26] It consists hydroxyl ions (OH^-) in its hexagonal structure and these OH^- ions may as well increase electrical conductivity as well as charge carrier capacity in the presence of required band gap energy. [27,28] Besides, PO_4 groups in the HAP surface generates O_2 Accept radicals during the photocatalytic process and these generated O_2 radicals may act as an electron receiver to attained the separation of electron-hole pairs.[29,30] Thus, it is expected that synthesis of HA/TiO_2 composite might enhance the optical properties, adsorption capability and also minimize the recombination of generated electron-hole pair during the photo catalysis process through appropriate and required

band gap energy. Therefore, despite all the aforementioned extensive investigation on the properties of HA/TiO_2 there are no reports on the study of optical properties of hydroxyapatite doped titanium dioxide: focus in band gap energy determination using three different models to the best of our knowledge. Hence, the present study is intended to analyzed the nature of optical constant of HA/TiO_2 at different percentage weight of hydroxyapatite (0wt%, 30wt%, 40wt%, 50wt%, 60wt%, 70wt% and 80wt%), thereby focusing on band gap energy determination using three different models. The models are Tauc, ASF (atomic spectrum fitting), DASF (Derivation of atomic spectrum fitting) in order to ascertain the exact, correct and precise method of band gap energy determination that could be able to excite a greater number of mobility carrier applicable for optoelectronic application. It was found that, the absolute magnitude of the optical gap as determined by the linear extrapolation in Tauc's and ASF procedures, is quite sensitive to the range over which the extrapolation is taken, according to [31], while DASF avoids this problem since the complete spectrum is fitted. Notwithstanding, the optical band gap in DASF method is obtained by taking the whole derivative of the spectrum instead of extrapolating certain range as in Tauc and ASF method. As a result, this makes DASF method exceptional, more efficient and accurate model for band gap determination.

Experimental Procedure

Materials

1.7244g per 20ml of TiO_2 solution, 4.311mg of HA per 2ml solution, glass slides of dimensions all of purity 99.9%, and glass slide plate of 2.5mm x 2.5mm Titanium (IV) isopropoxide [$C_{12}H_{28}O_4Ti$] (TTIP). serum plain micro point diagnostics vacuum tube. propanol, acetic acid and orthophosphoric acid [H_3PO_4]. Hence, calcium to phosphate ratio (ca/pa) was found to be 1.65 – 67.

Preparation of HAP/TiO_2 Composite Thin Film and Characterization.

Titanium (IV) isopropoxide [$C_{12}H_{28}O_4Ti$] (TTIP) of purity 99.99% was used as a source material for Titanium [Ti]. Propanol and double distilled water (dH_2O) were used as solvents and acetic acid was used as a stabilizing agent. The propanol, acetic acid and orthophosphoric acid [H_3PO_4] were obtained from solaronic. Microscopic glass slides of dimensions 2.5 mm × 2.5 mm were used as substrates. The substrates were washed with soap solution for 5 min and subsequently kept in a hot chromic acid at 50°C for 20 min. Finally, the substrates were cleaned ultrasonically and washed with distilled water. A prepared solution of HA/TiO_2 Nano composite were obtained by stoichiometric analysis of 1.7244g per 20ml of TiO_2 solution which contained 2930g is mixed together with proportion of 4.311mg of HAP per 2ml solution. By varying stoichiometrically the Wt% of HA (0, 30, 40, 50, 60, 70, and 80) wt% with a corresponding 20ml volume of TiO_2. To obtained the corresponding mass in grams of the HAP, we make used of the relationship

$$\frac{x}{4.311+x} = wt\%. \quad 1.0$$

Similarly for volume of TiO_2 we used $20\ X\ \frac{x}{2930}$ 2.0

After that, 20ml of TiO_2 propanol mixture suspension was added drop by drop in different percentage weight of HA mixture, and then, stirred vigorously for 2 h. Subsequently, the reaction mixture was ultra-sonicated (60W Bath sonicator, PCI Analytics) for another 4hr. Next, the reaction mixture was autoclaved for 8h at 190^{OC} and then, centrifuged at 6000 RPM for 20 min to collect the formed HA/TiO_2 composites. The TiO_2 film was deposited on the slide glass to fabricate a 4nm thick film, then the HA was coated to obtain a 4nm thickness. The total film thickness was 8nm. The film was annealed in air at 350^{OC} for 4 h in an electric furnace. The optical characterization was carried out using Thermo

scientific Evaluation 300 UV- vis absorption spectrophotometer. (300UV; Jasco corp., japan) were used.

Theories and Models for HA/TiO_2 Evaluation

From the absorption data, the optical constant such as absorption coefficient, extension coefficient and refractive index of the materials following the bellow relationship.

Recall that, the absorbance (A), is the ratio of intensity of light absorbed I_A by the sample to the incident intensity of light I_O.

$$A = I_A/I_O \quad 3.0$$

Transmittance T is given by

$$T = exp^{(-2.303A)} \quad 4.0$$

Reflectance R is calculated as

$$R = 1 - (A + T) \quad 5.0$$

The reflectance data was used to calculate the refractive index (n) of the thin film using equation

$$R = \frac{(n-1)2}{(n+1)2} \quad 6.0$$

$$n = \frac{1+\sqrt{R}}{1-\sqrt{R}} \quad 7.0$$

The extension coefficient (k) was calculated using the following equation

$$\bar{n} = n + ik \quad 8.0$$

Where n is the real part named as refractive index and k is the imaginary part named as extinction coefficient. Extinction coefficient provides information about the absorption of light in material medium due to inelastic scattering. It is known that extinction coefficient and absorption coefficient can be related by the following formula

$$k(\lambda) = \frac{\alpha(\lambda)\lambda}{4\pi} \quad 9.0$$

Where k(λ) is the extinction coefficient. The wavelength dependence of extinction coefficient of the thin films.

Models (Tauc, ASF and DASF)

Similarly, based on the absorption values, three different models (Tauc's, ASF, and DASF) were used to estimate the band gap energy of the synthesized HA/TiO_2. The popular method known as Taucs plot required both the data of absorbance and sample thickness at the UV-spectroscopy.

However, ASF and DASF models requires only the absorbance values HA/TiO_2 for band gap determination, hence the following theoretical approaches were used. In Taucs models the following relationship were used according to Davis and Mot to estimate the direct band gap energy of HA/TiO_2

$$\alpha(v)hv = B(hv - E_{HA/TiO2}^{TAUS})^{m} \quad 10.0$$

By re-arranging equation 15 to obtained

$$\alpha(hv)^{1/m} = B(hv - E_{HA/TiO2}^{Tauc})^{m} \quad 11.0$$

HA/TiO2 Tauc , B and hv are the HATiO_2 energy independent constant and incident photon energy, respectively. The exponent m can take the values 1/2, 2, 3/2, and 3, which respectively signify the direct allowed, indirect allowed, direct forbidden, and indirect forbidden optical transitions. The absorption coefficient α(v) according to the Beer–Lambert law takes the form

$$\alpha(v) = \frac{2.303 \times A}{t} \quad 12.0$$

where t and A are the thickness and absorbance of the glass sample, respectively. Transforming Tauc's relation in terms of the wavenumber and wavelength (λ), the optical absorption coefficient (α(λ)) can be obtained through the ASF relation according to [12.0].

$$\alpha(\lambda) = B(hc)^{m-1}\,\lambda\left(\frac{1}{\lambda} - \frac{1}{\lambda g}\right)^{m} \quad 13.0$$

where α(λ) is the absorption coefficient defined by the Beer–Lambert's law as:

$$\alpha(\lambda) = (2.303/z)\,A, \quad 14.0$$

TIJERAT
ISSN: 2707-5654

Considering z and A as film thickness and film absorbance, respectively, also, m is the index which can have different values 1/2, 3/2, 2, 3 [32] λg, h, and c are wavelength corresponding to the optical gap

$(E_{gap}^{ASF} = \frac{hc}{\lambda g}$ = 1239.83/λg), 15.0

Planck's constant and the velocity of the light, correspondingly. Using the Beer–Lambert's law, Eq.18 can be re-write as:

$$A(\lambda) = D\lambda\left(\frac{1}{\lambda} - \frac{1}{\lambda g}\right)^{m} \quad 16.0$$

where D = [B(hc) m^{-1} z/2.303]. 17.0

In ASF and Tauc's methods, one can determine m by examining the different m values and choosing the best fitted m value; so, using the optimized value of m, the optical gap can be obtained in ASF methods using equation 15.0

In this proposed method (DASF), Eq. 21 can be written as:

$$lnA\frac{(\lambda)}{\lambda} = \ln(D) + m\,ln\left(\frac{1}{\lambda} - \frac{1}{\lambda g}\right) \quad 18$$

and then:

$$\frac{d\left[\ln\left(\frac{A}{\lambda}\right)\right]}{d\left(\frac{1}{\lambda}\right)} = \frac{m}{\frac{1}{\lambda} - \frac{1}{\lambda g}} \quad 19$$

Plot of $d\left[\ln\left(\frac{A}{\lambda}\right)\right]$ Against $\frac{1}{\lambda}$ can be made to locate the expected discontinuity at $\frac{1}{\lambda} = \frac{1}{\lambda g}$

yields

$$E_{\frac{HA}{TiO2}}^{DASF} = \frac{hc}{\lambda g} = 1239.83/\lambda g \quad 20$$

The value of m (indicating the nature of optical carrier transition) were determined from the slope of the linear part of plot as can be seen in equation 21, and the value of m can be determine using equation 22

Ln[A(λ^{-1}) versus Ln(λ^{-1}−λ_g^{-1}) 21

The slope was achieved by $m = \frac{\Delta \ln A(\lambda^{-1})}{\Delta Ln(\lambda^{-1} - \lambda_g^{-1})}$ 22

Which gives the exact values of m^{DASF} for various material

TIJERAT
ISSN: 2707-5654

Results and Discussion.

Optical characterization.

It was reported that, the absorption spectrum of semiconductor directly determines the electronic structure of the material by exciting electrons from the valence band to the conduction band using ultraviolet and visible radiation. Hence, Fig.2.0 depict the optical absorption spectra of HA/TiO_2 composite thin films with a percentage weight (wt%) of 0, 30, 40, 50, 60, 70, 80, recorded in the spectrum of wavelength ranging from 400 nm - 1200 nm. It was observed clearly, that the strong response in the UV region is shown at 200 nm–400 nm, with an absorption edge around 650nm–950 nm. The reason for the absorption edges of HA/TiO_2 at 650 nm is due to the charge transfer from the valence band to the conduction band of the Ti^{4+} cations, as a result of enhancement of HA/TiO_2 films compactness (shrinkage of the bond length). This is in agreement with research done by [32]. Here it is clearly showed that, the absorption band corresponding to the HA/TiO_2 Nano composites gets blue shifted, the shift of the absorption band towards shorter wavelength indicates decrease in particle size, while the absorption edges get red shifted indicating an increase in the particles size of HAP that are active in TiO_2 layer, which is also consistent with the result of [32]. Figure3.0 is the optical transmittance of HA/TiO_2 at different weight percentage, which was obtained using equation 5.0. It was observed that, at 0wt% the transmittance is at maximum greater than 95% in the visible light region (400 – 800) nm due to 0wt% of HAP particles on TiO_2, negligible wt% of HAP particles which in turns leads to small particles size, and this create more avenue for high transmittance capacitance at 0wt% of HA/TiO_2 film. Conversely, spectra transmittance sharply decreased at the UV region as the wt% of HAP increased, hence an obvious absorption edge was observed at 680 nm, this could be as a result of increased in percentage weight of HAP on TiO_2 which in turn gives larger particle size that will trap the UV- light thereby reduce the degree of transmittance in HA/TiO_2 this

is in accordance with the result of [33]. After subsequent percentage weight of HA on TiO_2 and moderate heat treatment, the transmittance of the HA/TiO_2 film decreased by around 8% in the visible light region. This is because the crystal grain grows by heat energy. In addition, it was reported by [33] that the grain size of TiO_2 film increased with annealing temperature from an atomic force microscopy observation, and the transmittance of the film decreased.

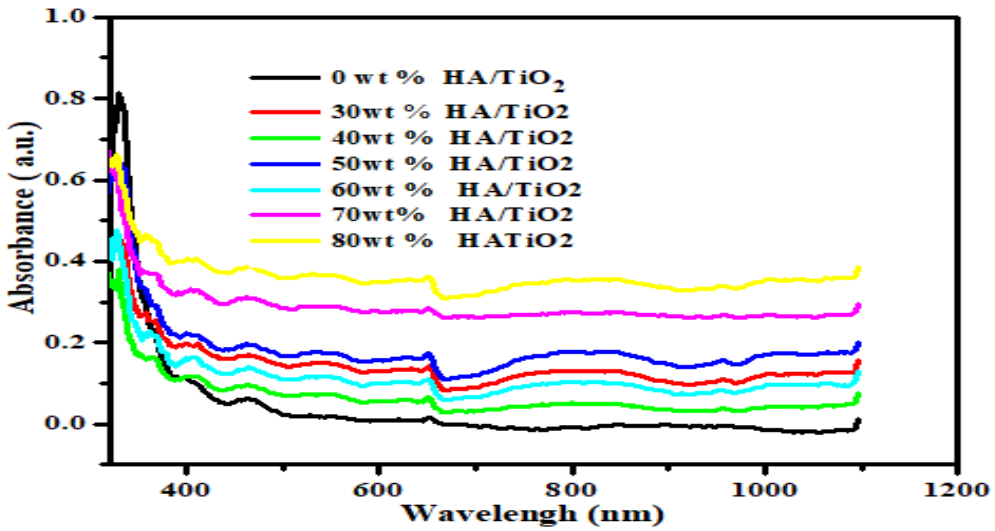

Figure 3.0 optical absorbance of HA/TiO_2 at different percentage weight.

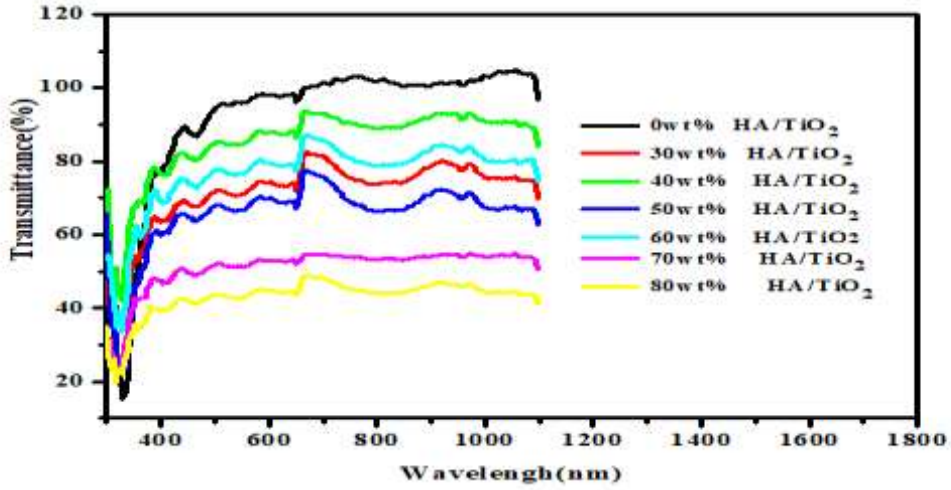

Figure 3.1 optical transmittance of HA/TiO_2 at different percentage weight.

Optical Constant of HA/TiO_2

Absorption coefficient, Extension coefficient and Refractive index.

Figure 3.2 illustrate the variation of absorption Coefficient with Wavelength at different wt% of HA, at a wavelenght ranging from 300nm – 1200nm, and it was evaluated using equation 9.0 From figure 3.2 it was observered that as the wt% of HA increases in TiO_2 the absorption also increases except at 0wt% and 40wt% which shows an abnormality with a greater absorption coefficient value, this could be as a result of absence or little percentage of hydroxyapatite nanoparticles which could disperse homogeneously in the matrix with sufficient TiO_2 proportion and greatly reduce the agglomeration effect of the hydroxyapatite nano particles; hence promoting the absorption coefficient with little or no HA nanoparticles, which is in line with the result of [34]. Figure 3.3 displayed the extension coefficient (k), of HA/TiO_2 at different wt% of HA, it was evaluated using equation 9.0 from absorbance data. It is clearly shown that, the extension coefficient is high at 0wt% and low at 40wt% of HA, and it was found increasing with increased in wt% of HA up (80wt %). The small wt% of HA indicates that, the composite samples are still transparent to electromagnetic radiation, thereby increase the extension coefficient, this is in accordance with the other researcher such as [36]. The variation in the refractive index (n) and extension (k) values HA/TiO_2 with the wavelength reveals that some interaction takes place between photon and electrons of the films. Furthermore, increase in values of extension coefficient (k) at high wavelength for wt% of HA, indicates scattering of more photon with added quantity of HA, this agreed with the result of [37]. The values of absorption coefficient (α) and extension coefficient (k) of HA/TiO_2 at a particular wavelength of 300nm are observed in figure 3.2 & figure 3.3. These values show an increasing trend on increasing the wt% of HA. This is in accordance with work of [37,38]. Figure 3.4 depict the dispersion in refractive index (n) for different doped HA/TiO_2 at invested range of wavelength from

300nm – 1200nm, which were evaluated from the absorbance values using equation 7.0. Figure 3.4 indicate that, the refractive index (n), increases with increasing %wt of HA thin films up 0.325 in HA/TiO_2 and the increase in the dispersion of thin films occurs at 0wt% HA/TiO_2. However, highest refractive index occurs at 0wt% and the lowest occurs at 40wt% HAP with a high wavelength value respectively. The increase and decrease in refractive index (n) with increasing wt% of HA/TiO_2, indicates that the refractive index (n) is tunable upon addition of different wt% of HA on a substrate, this is in accordance with the work of [39]. From the below figure 3.4.0 it could be noticed that, the refractive index decreases abruptly as the wavelength increases and gets saturated beyond the wavelength of 1000 nm. The high wavelength region of refractive index (n) represents the materials bulk properties. The sudden increased of refractive index (n) for TiO_2 volume and wt% of HA may be attributed to the percolation threshold phenomenon; this is in agreement with [39].

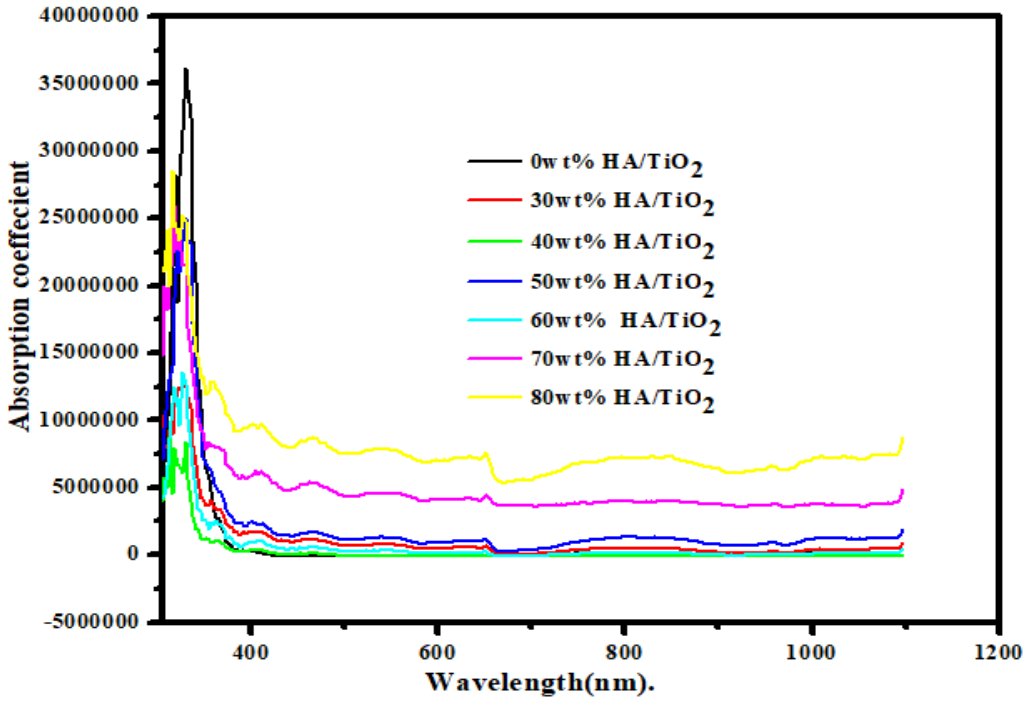

Figure 3.2 Variation of Absorption Coefficient of HA/TiO_2 with Wavelength at different wt% of HA.

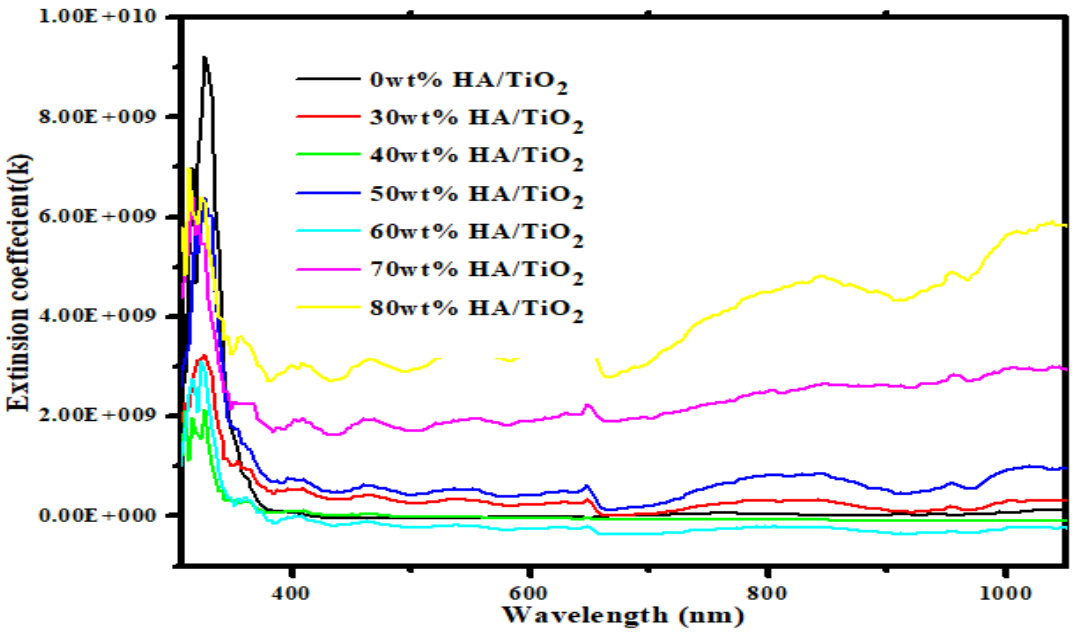

Figure 3.3 Variation of Extension coefficient (k) of HA/TiO_2 with wavelength at different wt% of HA.

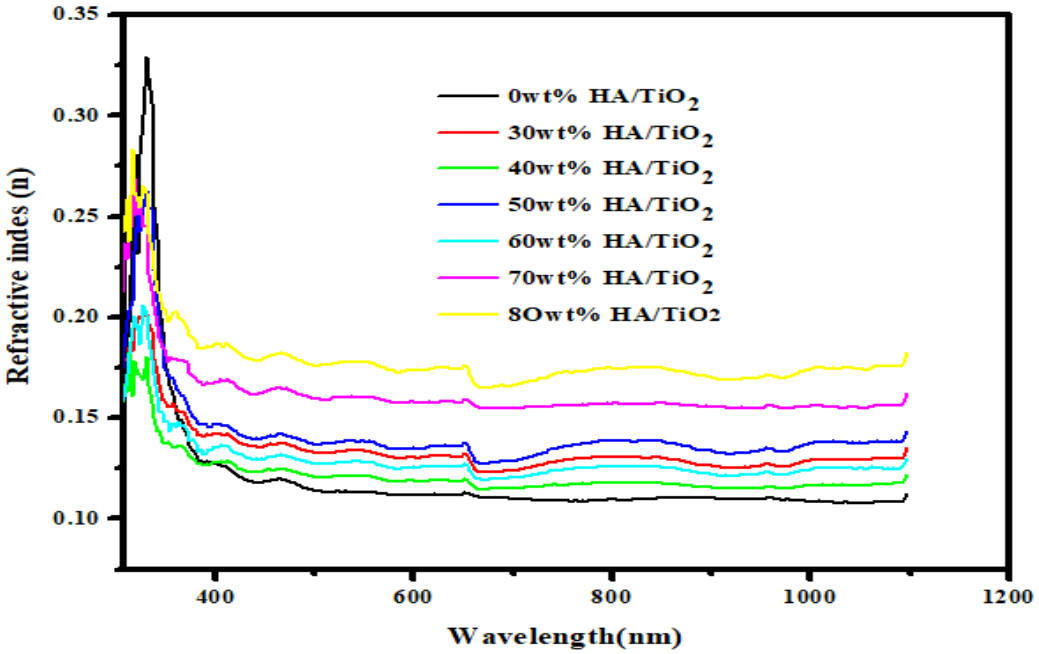

Figure 3.4.0 Variation of Refractive index(n) with Photon Energy of HA/TiO_2 at different wt% of HA

Optical Band Gap Energy Using Three Different Models (Tauc, ASF and DASF)

Tauc Model

Figure 3.5 displayed the Tauc method for band gap determination of HA/TiO_2 at different percentage weight of hydroxyapatite (wt%). The band gap energy is obtained by extrapolating the linear portion of a curve and intersecting it with the horizontal axis, there by estimating an appropriate value for each percentage weight of HA using equation 16, and the value of estimated band gap energy is shown in table 1.0. The analysis proved that, at 0wt% and 30wt% HA/TiO_2 the band gap energy has an estimated value of 3.61eV and 3.57eV. In addition, at 40wt%, 50wt% and 60wt% the observed value of band gap energy at each point is 3.51eV, 3.38eV, and 3.56eV respectively. From the above analysis, its clearly shown that, the band gap of a materials decreases as the percentage weight of hydroxyapatite increases within a range of (3.61 – 3.25) eV, except at 60wt% which has an increase in the band gap value of about 3.56eV. The lower value of E_g is attributed to the creation of allowed energy states in the band gap [44,45] as a result of increase in particles size at the time of film preparation, while the higher value of E_g is accounted to the very small grain size of the film leading to an increase in the grain boundary, hence increase in the band gap energy. This is in agreement with the research conducted by [44,45].

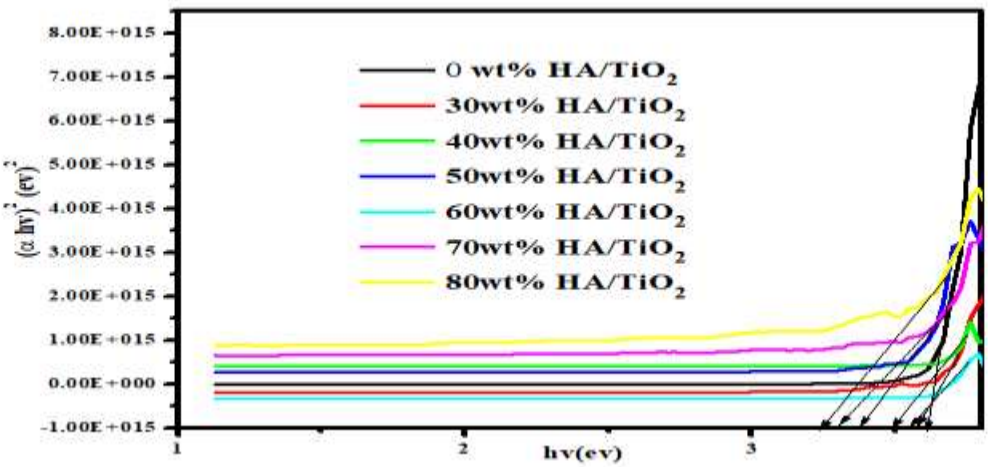

Figure 3.5 Variation of $(\alpha hv)^2$ $(ev)^2$ against hv(ev) optical bandgap of HA/TiO_2 at different HA wt% using Tauc mode

Table 1.0 Optical bandgap values for three different models and their type of transition.

Sample wt%	0 HA/TiO_2	30 HA/TiO_2	40 HA/TiO_2	50 HA/TiO_2	60 HA/TiO_2	70 HA/TiO_2	80 HA/TiO_2
Tauc model E_{Direct}^{Taus} E_g(ev)	3.61	3.57	3.51	3.38	3.58	3.25	3.22
ASF model E_{Direct}^{ASF} E_g(ev)	3.22	3.25	3.24	3.22	3.24	3.24	3.22
m^{ASF} $\pm$0.01	$\frac{1}{2}$	$\frac{1}{2}$	$\frac{1}{2}$	$\frac{1}{2}$	$\frac{1}{2}$	$\frac{1}{2}$	$\frac{1}{2}$
DASF model E_{Direct}^{DSF} E_g(ev)	3.11	3.09	3.09	3.09	3.11	3.11	3.09
m^{DASF} $\pm$0.01	1.24	1.26	1.25	1.27	1.27	1.27	1.27

ASF (Atomic Spectrum Fitting) Model

Figure 3.6 depicted an ASF method for band gap determination at different wt% of HA on TiO_2. To estimate the value of the band gap energy using these model, a plot of $(A/\lambda)^2$ versus λ^{-1} (nm^{-1}) were established using equation 13.0, assuming that the transition is a direct one and a linear fit was made. The band gap energy Eg was obtained from the intercept with the λ^{-1} (nm^{-1}) axis, by substituting the value of λ^{-1} (nm^{-1}) in each case in equation 15.0 yield the exact value of band gap energy at each wt% of HA/TiO_2. Hence from the above analysis, its observed that in figure 3.6 (a

& b) with 0wt% and 30wt% of HAP has a band gap energy value of 3.22eV and 3.25eV. Thereafter, as the percentage weight of HA increases to 40wt%, 50wt% and 60wt% as displayed in figure 3.6 (c, d & e) the estimated value of band gap energy was observed to be 3.24eV, 3.22eV, and 3.24eV respectively. In general, the band gap energy value is at the range of (3.22 – 3.24) eV at (0 – 40) wt% HA shown in figure 3.6 (a, b, and c), similarly (d, e, f and g) the band gap energy ranging from (3.22 – 3.22) eV. This shows clearly that, there is slight increase in the band gap energy and then it became constant as the percentage weight of hydroxyapatite increases. The increase in wt% of HA lead to an increase in the film thickness. However, slight increase in the optical band gap is attributed to the improvement in the crystallinity of the films when they become thicker, because the crystallinity of the film also increases due to the increase in crystallite size which account for the decrease in the band gap. This is in line with the research done by [45].

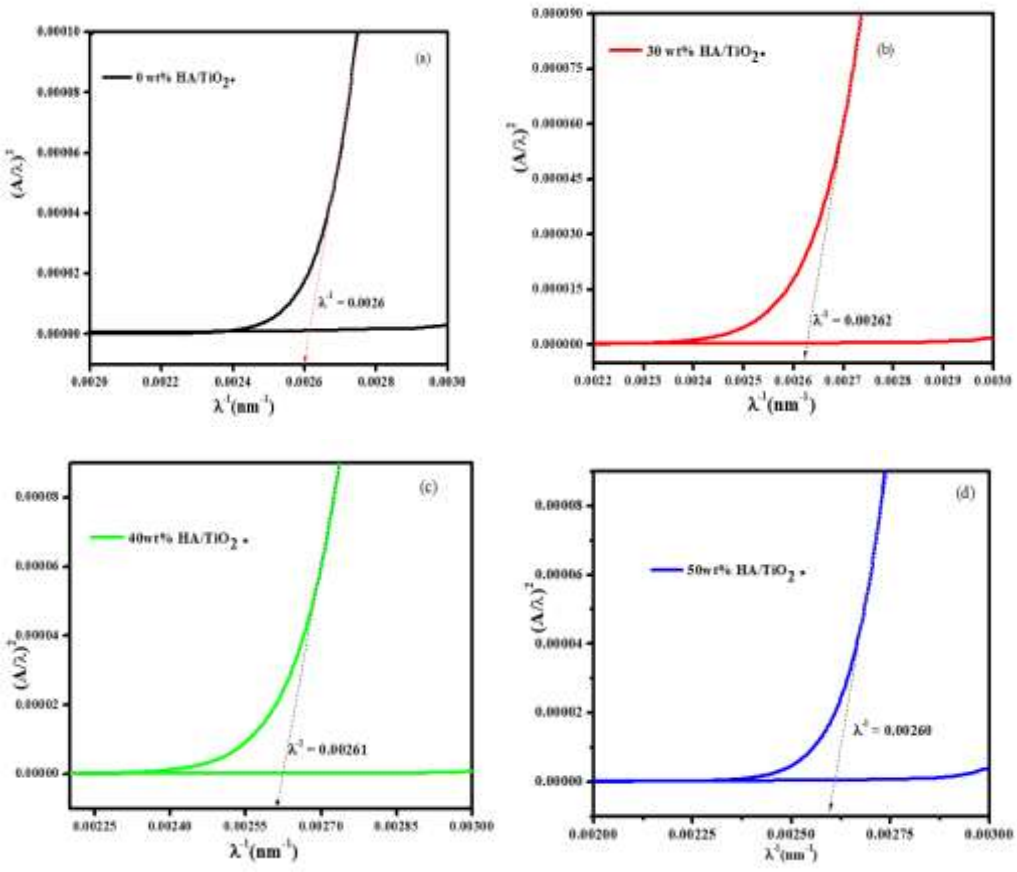

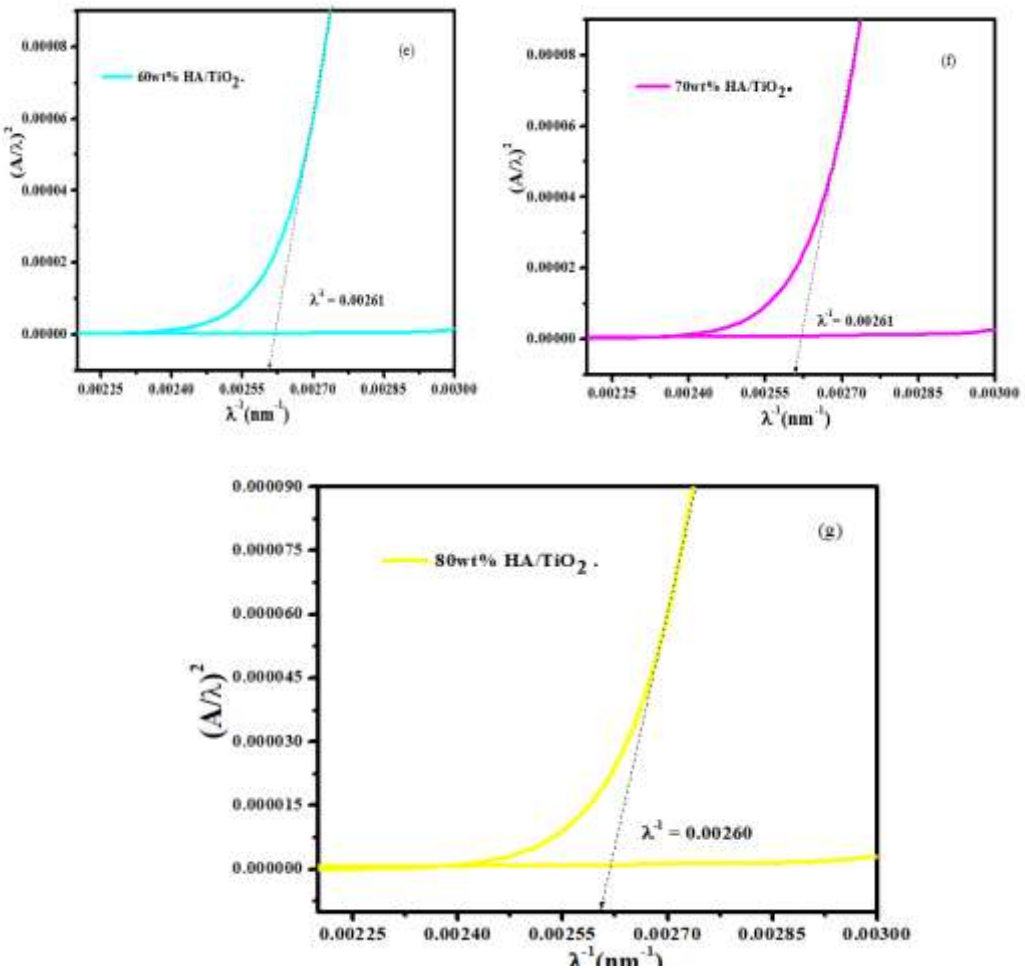

Figure 3.6 Variation of $(A/\lambda)^2$ versus λ^{-1} (nm^{-1}) Bandgap energy of HA/TiO_2 at different HA wt% (a) 0HAwt% (b) 30wt% (c) 40wt% (d) 50wt% (e) 60wt% (f) 70wt% (g) 80wt%. Using ASF models.

3.1.5 DASF (Derivation of Atomic Spectrum Fitting) Model

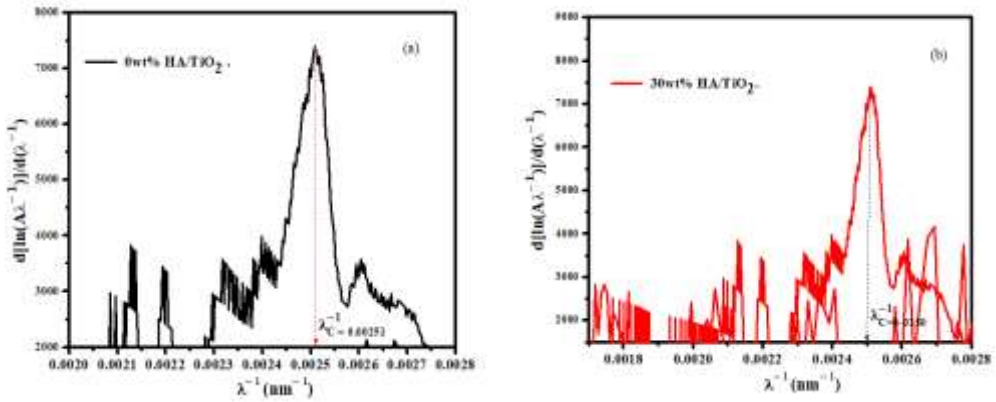

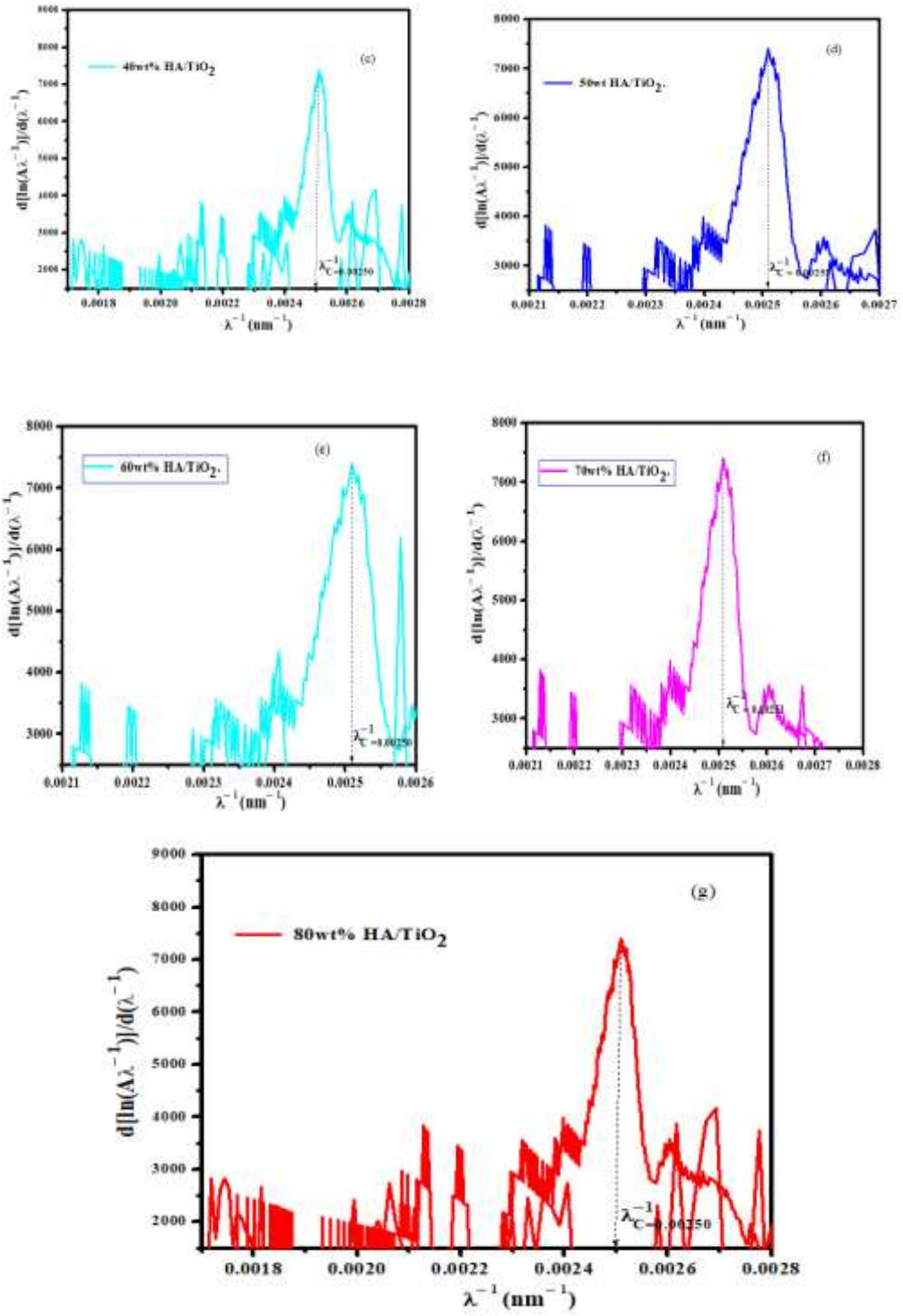

Figure 3.7 Variation of d{ln [A(λ)/λ]}/ d(1/λ) versus λ^{-1} (nm^{-1}) Bandgp energy of HA/TiO_2 at different HA wt% (a) 0HAwt% (b) 30wt% (c) 40wt% (d) 50wt% (e) 60wt% (f) 70wt% (g) 80wt%. Using DASF models.

From the above Figure 3.7, is the DASF method for optical band gap determination at different wt% of HA/TiO_2. To estimate the value of the band gap energy using DASF model, a plot of d{ln [A(λ)/λ]}/ d(1/λ) versus λ^{-1} (nm^{-1}) were established in equation 18.0 starting from ASF model, without any presumption about the type of transition, rather it involves a complete spectrum fitting techniques. Hence, the band gap energy Eg was obtained from the intercept with the λ^{-1} (nm^{-1}) axis, by substituting the value of λ^{-1} (nm^{-1}) in each case in equation 20.0 yield the exact value of band gap energy at each wt% of HAP on TiO_2. Therefore, from the above prediction, in figure 3.7 (a, b, and c) the band gap energy value was calculated to be 3.11eV, 3.09eV and 3.11eV. Moreover, as the percentage weight of HA increases as showed in figure 3.7 (d, e and f) the estimated value of band gap energy was observed to be 3.11eV, 3.09eV, and 3.11eV respectively. Finally, in figure 3.7 (g) the band gap energy was found to be 3.09eV at 80wt% HAP. In these models, the band gap energy value slightly decreases at a specific range of (3.11 – 3.09) eV at (0 – 40) wt% HAP as depicted in figure 3.7 (a, b, and c), likewise in the same figure (d and e) at 50wt%, 60wt% also in (f and g) at 70wt%, 80wt% there was a negligible increased and decreased in the band gap energy values of 3.11eV, 3.09eV and 3.11eV, 3.09eV respectively, showing an infinitesimal band gap different values of 0.02eV which absolutely indicate a complete spectrum fitting techniques. Further investigation shows that addition of HAP causes breaking of the regular structure of hydroxyapatite and titanium dioxide leading to a decrease in the band gap, this agreed with the result of [47]. In addition, this decreasing is due to an increase in the disorder and consequently the more extension of the localized states within the gap as a result of increase in the percentage weight, which is in accordance with the findings of [48]. Hence, from the above findings it is clearly shown that, the values obtained from DASF model is more precise and accurate than Tau's and ASF models. Figure 3.8 displayed the method of how the optical

transitions were determined at different weight percentage of hydroxyapatite. The value of m (optical transition) was determined from the slope of the linear part of $\ln(A\lambda^{-1})$ versus λ^{-1}-λ_g^{-1} plots and were estimated using equation 28, This method helps us to calculate m values for all the film studied here without any presumption of the nature of transition, the obtained values are found in table 1.0. All the transition values are varied within the range of 1.24 – 1.27 for different wt% of HA/TiO_2 and are approximately almost about 1/2, which disclosed direct allowed transition; this result is in good agreement with the optimum m value obtained from ASF for the present samples, and its agreed with the result obtained by [49]

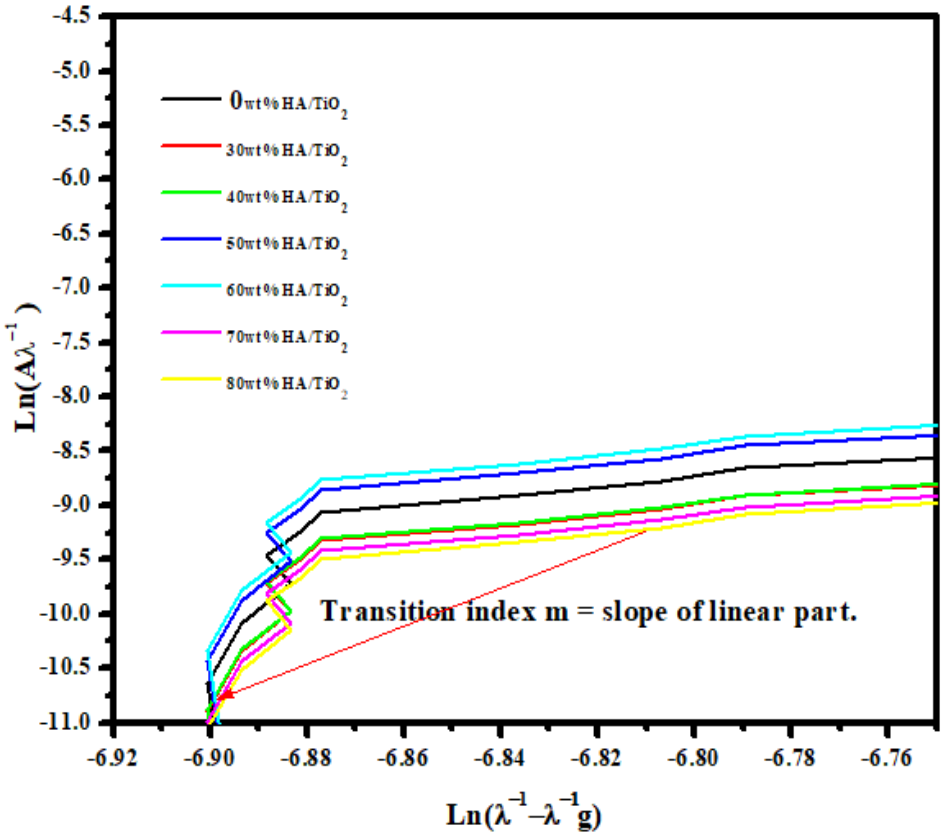

Fig. 3.8 DASF plot indicating the nature of optical transition (m) in the HA/TiO2 thin film.

Conclusions

In this work, a new method (called DASF) was proposed and described easily and rapidly obtained the optical properties of HA/TiO_2, focus on band gap determination using three different model, and the nature of optical transitions. The main advantages of the DASF method are: (a) avoiding the film thickness measurement, (b) only measurement of the film absorbance is enough and (c) no any presumption of the nature of optical transition and no any need to linear extrapolation. Hence the methods were evaluated through HA/TiO_2 synthesizes and analysis. In general, it was discovered that the optical parameter such as transmittance, absorbance, absorption coefficient, extision coefficient and refractive index, tend to increase as the percentage weight of HA increases. The values of the band gap obtained using ASF and DASF analysis methods were compared, and found to be in a good agreement and similar trends was observed, unlike Taucs model where large disparity in the values was noticed. In DASF optical band gap energy determination, the maximum value was found to be 3.11 eV at 80wt% of HAP and the minimum value equal to 3.09 eV at 0wt%, and in Tauc model, the maximum band gap energy was also observed at 3.61eV, while in ASF model there was increase and decrease in the energy gap with a range between (3.22 – 3,25) eV.

Acknowledgements

One of the authors T Yunana, sincerely appreciate the sheda science and technology Abuja, also thanks goes to Nigerian Defence Academy kaduna staffs for their patient and kind supervision during the laboratory investigation. Thanks the kaduna state government for providing financial assistance to carried out the whole analysis.

REFERENCES.

[1]. V, Maurice, T, Georgelin, JM, Siaugue, Cabuil VSynthesis and characterization of functionalized core-shell gamma Fe_2O_3-SiO_2 nanoparticles. Journal of Magnetism and Magnetic Materials;321(10). (2009) 1408–1413.

[2]. H, Bala Y, Zhang Yang H, Wang C, Li M, Lv X, Z Wang Preparation and characteristics of calcium carbonate/silica nanoparticles with core-shell structure. Colloids and Surfaces A.294(1) (2007) 8–13.

[3]. M, Okada Y, Yamada P, Jin M, Tazawa K, Yoshimura. Fabrication of multifunctional coating which combines low-e property and visible-light-responsive photocatalytic activity. Thin Solid Films.;442(1) (2003) 217-221.

[4] A, Ennaoui BR, Sankapal V, Skryshevsky MC, Lux-Steiner. TiO_2 and TiO_2-SiO_2 thin films and powders by one-step soft-solution method: Synthesis and characterizations. Solar Energy Materials and Solar Cells.90(10) (2006) 1533-1541.

[5]. R, Weinberger RB, Garber.Titanium-dioxide photocatalysts produced by reactive magnetrón sputtering. Applied Physics Letters. 66(18) (1995) 2409-2411.

[6]. D, Manno G, Micocci R, Rella A, Serra A, Taurino A, Tepore . Titanium oxide thin films for NH3 monitoring: Structural and physical characterizations. Journal of Applied Physics. 82(1) (1997) 54-59.

[7]. A, Ramadoss SJ, Kim. Vertically aligned TiO_2 nanorod arrays for electrochemical super capacitor. Journal of Alloys Compounds.561(2013) 262-267

[8]. J, Seo J, Jeong and C, Lee Photocatalytic degradation of organic compounds by 2-ethylimidazole-treated titania under visible light illumination. Membr. Water Treat., 10(3) (2019) 223–9

[9]. S, Mozia P, Sienkiewicz K, Szymański M, Zgrzebnicki D, Darowna A, Czyżewski and Morawski AW, Influence of Ag/titanate nanotubes on physicochemical, antifouling and antimicrobial properties of mixed-matrix polyethersulfone ultrafiltration membranes. J. Chem. Technol. Biotechnol., 94(8) (2019) 2497-2511

[10].AT, Kuvarega N, Khumalo D, Dlamini , and BB Mamba. Polysulfone/N,Pd co-doped TiO_2 composite membranes for photocatalytic dye degradation. Sep. Purif. Technol., 191(2018) 122–133.

[11]. SN Hoseini AK, Pirzaman MA, Aroon AE, and Pirbazari, Photocatalytic degradation of 2,4-dichlorophenol by Co-doped TiO_2 (Co/TiO_2) nanoparticles and Co/TiO_2 containing mixed matrix membranes. J. Water Process Eng., 17(2017) 124–134.

[12]. S, Teixeira H, Mora LM, Blasse PM, Martins SAC, Carabineiro S, Lanceros-Méndez S, K, Kuhn and CunibertiPhotocatalytic degradation of recalcitrant micro pollutants by reusable Fe_3O_4/SiO_2/TiO_2 particles. J. Photochem. Photobiol. A Chem., 345 (2017) 27–35.

[13]. G, Boopathy A, Gangasalam and A, Mahalingam Photocatalytic removal of organic pollutants and self-cleaning performance of PES membrane incorporated sulfonated graphene oxide/ZnO nanocomposite. J. Chem. Technol. Biotechnol., 91 (10) (2020).6462.

[14] G. Shukla, P.K. Mishra, A. Khare, Journal of Alloys Compound. 489 (2010) 246–251.

[15] H. Ogawa, T. Higuchi, A. Nakamura, S. Tokita, D. Miyazaki, T. Hattori, T. Tsukamoto, Journal of. Alloys Compound. 449 (2008) 375–378.

[16] A.K. Srivastava, M. Deepa, S. Bhandari, H. Fuess, Nanoscale Res. Lett. 4 (2009) 54–62.

[17] I. Hotovy, A. Pullmannova, M. Predanocy, J. Hotovy, V. Rehacek, T. Kups, L. Spiess, J Electr. Eng. 60 (6) (2009). 354–357.
[18]. W.D. Brown, W.W. Grannemann Solid State Electron. 21, (1978) 837–846
[19] J.D. Fidelus, M. Barczak, K. Michalak, Z. Fekner, A. Duzynska, A. Jusza, R. Piramidowicz, C.J. Monty, A. Suchocki, J Nanosci. Nanotechnol. (12) (2012) 3760–3765.
[20] H, Liu T, Lv C, Zhu and Z, Zhu Direct bandgap narrowing of TiO_2/MoO_3 heterostructure composites for enhanced solar-driven photocatalytic activity. Sol. Energy Mater. Sol. Cells, 153(2016). 1–8.
[21].D, Friedmann C, Mendive and D, Bahnemann TiO_2 for water treatment: Parameters affecting the kinetics and mechanisms of photocatalysis. Appl. Catal. B Environ., 99 (3–4) (2010) 398–406.
[22]. M, Gar Alalm A, Tawfik and S, Ookawara . Enhancement of photocatalytic activity of TiO_2 by immobilization on activated carbon for degradation of pharmaceuticals. J. Environ. Chem. Eng., 4 (2) (2016). 1929–1937
[23]. MR, Eskandarian M, Fazli MH, Rasoulifard and H, Choi Decomposition of organic chemicals by zeolite-TiO_2 nanocomposite supported onto low density polyethylene film under UV-LED powered by solar radiation. Appl. Catal. B Environ., 183(2016) 407–416
[24] J, Matos J, Laine and JM Herrmann, Effect of the type of activated carbons on the photocatalytic degradation of aqueous organic pollutants by UV-irradiated titania. J. Catal., 200 (1) (2001) 10–20.
[25].A, Pal TK, Jana, and K, Chatterjee, Silica supported TiO_2 nanostructures for highly efficient photocatalytic application under visible light irradiation. Mater. Res. Bull., 76 (2016) 353–357.
[26]. M, Cui, S, Pan Z, Tang X, Chena X, Qiao and Q, Xu. Physiochemical properties of n-n heterostructured TiO_2/Mo-TiO_2 composites and their photocatalytic degradation of gaseous toluene. Chem. Speciat. Bioavailab., 29 (1) (2017) 60–69.
[27]. M, Buchi Suresh P, Biswas V, Mahender R, and Johnson, Comparative evaluation of electrical conductivity of hydroxyapatite ceramics densified through ramp and hold, spark plasma and post sinter Hot Isostatic Pressing routes. Mater. Sci. Eng. C, 70 (2017) 364–370.
[28].JP, Gittings CR, Bowen Dent ACE, IG,Turner FR, Baxter and JB, Chaudhuri Electrical characterization of hydroxyapatite-based bioceramics. Acta Biomater., 5 (2), (2009). 743–754
[29]. H, Nishikawa, Surface changes and radical formation on hydroxyapatite by UV irradiation for inducing photocatalytic activation, J. Mol. Catal. A Chem., 206 (2003) 331–338
[30].Y, Chai J, Ding L, Wang Q, Liu J, Ren, and WL, Dai, Enormous enhancement in photocatalytic performance of Ag_3PO_4/HAp composite: A Z-scheme mechanism insight. Appl. Catal. B Environ., 179 (2015). 29–36.
[31], D, Souri · Z, Esmaeili Tahan, A new method for the determination of optical band gap and the nature of optical transitions in semiconductor. Journal of applied science. Vol, 10(6), (2015) 1103–1108
[32]. Kaviyarasub, Mariappana, K. Neyvasagamd, A. Ayeshamariame, P. Pandi d, R. Rajeshwara Palanichamyg, C. Gopinathanf , Genene T. Mola h, M. Maaza. Articles

on Photocatalytic performance and antimicrobial activities of HAp-TiO_2 nanocomposite thin films by sol-gel method. 8, (2016) 154 – 168

[33] D, Hou, M. Zhuang, G. Zhang, M. Zhao, M.-S. Wu, Applied. Surface. Science. 218 (2003) 97

[34] A, Balamurugan G, Balossier J, Michel JMF, FerreiraElectrochemical and structural evaluation of functionally graded bioglass-apatite composites electrophoretically deposited onto Ti6 Al4 V alloy. Electrochimica Acta. ; 54 (2009) 1192-1198

[35] Kaviyarasub, Mariappana, K. Neyvasagamd, A. Ayeshamariame, P. Pandi d, R. Rajeshwara Palanichamyg, C. Gopinathanf , Genene T. Mola h, M. Maaza. Articles on Photocatalytic performance and antimicrobial activities of HAp-TiO_2 nanocomposite thin films by sol-gel method. 8 (2016) 154 – 168.

[36] A, Balamurugan G, Balossier J, Michel JMF, Ferreira. Electrochemical and structural evaluation of functionally graded bioglass-apatite composites electrophoretically deposited onto Ti6 Al4 V alloy. Electrochimica Acta. ; 54 (2009) 1192-1198

[37] M, Nishikawa W, Yang Y, Nosaka Grafting effects of Cu_2+ on the photocatalytic activity of titanium-substituted hydroxyapatite. Journal of Molecular Catalysis A: Chemical. 378 (2013) 314-318

[38] M, Nishikawa W, Yang Y, Nosaka Grafting effects of Cu_2+ on the photocatalytic activity of titanium-substituted hydroxyapatite. Journal of Molecular Catalysis A: Chemical.;378(2013) 314-318

[39] M, Nishikawa W, Yang Y, Nosaka . Grafting effects of Cu_2+ on the photocatalytic activity of titanium-substituted hydroxyapatite. Journal of Molecular Catalysis A: Chemical.; 378(2013) 314-318

[40] A,Yakuphanoglu, I, Cukurovali, Yilmaz, Optical parameters induced by phase transformation in RF magnetron sputtered TiO_2 nanostructured thin film journal of Optical. Materials science. 27 (2005) 1366–1368

[41] MA, Aramendia,J, Hidalgo-Carrillo J, Sebti A study on the potential application of natural phosphate in photocatalytic processes. Journal of Colloid and Interface Science.;344(2) (2010) 475-481

[42] MA, Aramendia J, Hidalgo-Carrillo J, Sebti A study on the potential application of natural phosphate in photocatalytic processes. Journal of Colloid and Interface Science.;344(2) (2010) 475-481

[43] T, Nonami H, Hase K, Funakoshi Apatite-coated titanium dioxide photocatalyst for air purification. Catalysis Today. ;96 (2004) 113-118

[44] PP,Sahay RK, Nath S, Tewari Optical properties of thermally evaporated CdS thin films. Crystals Res Technology 42 (2007) 275–80.

[45] PP,Sahay RK, Nath S, Tewari. Optical properties of thermally evaporated CdS thin films. Cryst Res Technology42 (2007) 275–80.

[46] ER, Shaaban N, Afify A, El-Taher. Effect of film thickness on microstructure parameters and optical constants of CdTe thin films. *Journal of Alloys Compound* 482 (2009) 400–4190

[47] D, Souri · Z, Esmaeili Tahan, A new method for the determination of optical band gap and the nature of optical transitions in semiconductor. *Journal of applied science.* Vol, 10(6) (2009) 1103–1108

[48] N.P Mott, EA, Davis, Electronic process in non-crystalline materials (Clarendon Press, Oxford. (1979)

[49] D, Souri · Z, Esmaeili Tahan, A new method for the determination of optical band gap and the nature of optical transitions in semiconductor. *Journal of applied science.* Vol, 10(6), (2015). 1103–1108